Joule

Article

Enhancing charge-emitting shallow traps in metal halide perovskites by >100 times by surface strain

Graphical abstract

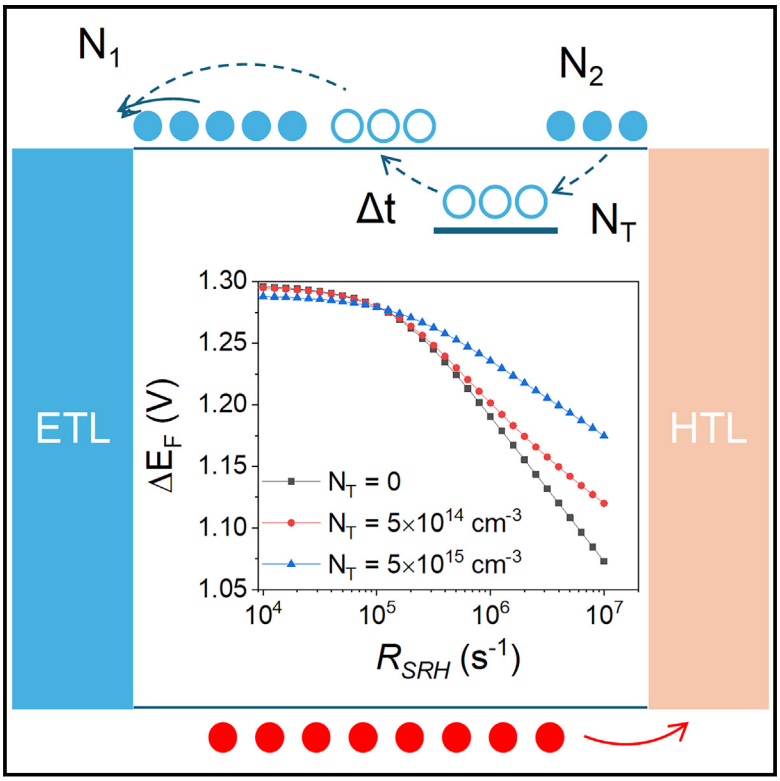

Highlights

- Much richer shallow traps in perovskites than traditional semiconductors
- Shallow traps density can be increased by surface microstrain by >100 times
- High-density shallow traps boost the open-circuit voltage of solar cells
- Reducing V_{OC} loss of perovskite photovoltaics to 317 mV by introducing shallow traps

Authors

Ying Zhou, Hengkai Zhang, Yeming Xian, ..., Farida A. Selim, Yanfa Yan, Jinsong Huang

Correspondence

jhuang@unc.edu

In brief

Shallow traps in perovskite have been applied to explain the observed extremely long carrier recombination times of perovskite films. However, the fundamental properties of shallow traps in perovskites are barely known. Herein, we directly characterized shallow traps in perovskite solar cells and found that perovskites have much richer shallow traps than traditional semiconductors. The shallow traps mainly locate on the film surface and can be enhanced by >100 times by introducing surface strain.

Zhou et al., 2025, Joule 9, 1–11
January 15, 2025
https://doi.org/10.1016/j.joule.2024.10.004

CellPress

Please cite this article in press as: Zhou et al., Enhancing charge-emitting shallow traps in metal halide perovskites by >100 times by surface strain, Joule (2024), https://doi.org/10.1016/j.joule.2024.10.004

Joule

CellPress

Article

Enhancing charge-emitting shallow traps in metal halide perovskites by >100 times by surface strain

Ying Zhou,[1,6] Hengkai Zhang,[1,6] Yeming Xian,[2] Zhifang Shi,[1] Jean Noalick Aboa,[3] Chengbin Fei,[1] Guang Yang,[1] Nengxu Li,[1] Farida A. Selim,[4] Yanfa Yan,[2] and Jinsong Huang[1,5,7,*]

[1]Department of Applied Physical Sciences, University of North Carolina at Chapel Hill, Chapel Hill, NC 27599, USA
[2]Department of Physics and Astronomy and Wright Center for Photovoltaics Innovation and Commercialization, The University of Toledo, Toledo, OH 43606, USA
[3]Department of Physics and Astronomy, Bowling Green State University, Bowling Green, OH 43403, USA
[4]School for Engineering of Matter, Transport and Energy, Arizona State University, Tempe, AZ 85287, USA
[5]Department of Chemistry, University of North Carolina at Chapel Hill, Chapel Hill, NC 27599, USA
[6]These authors contributed equally
[7]Lead contact
*Correspondence: jhuang@unc.edu
https://doi.org/10.1016/j.joule.2024.10.004

CONTEXT & SCALE Shallow traps in perovskite have been applied to explain the extremely long carrier recombination lifetime. However, the fundamental properties of shallow traps are barely known. Herein, we directly characterized shallow traps in perovskite solar cells and found that perovskites have much richer shallow traps than traditional semiconductors. The shallow trap density in perovskite can be enhanced by >100 times by introducing surface strain, which indicates that the shallow traps are mainly located at the film surface. The high-density shallow traps can temporarily hold electrons and increase free-hole concentration by keeping them from bimolecular recombination, reducing the V_{OC} loss of a very stable formamidinium-caesium (FACs)-perovskite to 317 mV. The investigation of open-circuit voltage can be enhanced by intentionally increasing the density of shallow traps, which brings a new strategy for further enhancing the perovskite solar cells efficiency.

SUMMARY

The low density of deep trapping defects in metal halide perovskites (MHPs) is essential for high-performance optoelectronic devices. Shallow traps in MHPs are speculated to enhance charge recombination lifetime. However, chemical nature and distribution of these shallow traps as well as their impact on solar cell operation remain unknown. Herein, we report that shallow traps are much richer in MHPs than traditional semiconductors, and their density can be enhanced by >100 times through local surface strain, indicating that shallow traps are mainly located at the surface. The surface strain is introduced by anchoring two-amine-terminated molecules onto formamidinium cations, and the shallow traps are formed by the band edge downshifting toward defect levels. The high-density shallow traps temporarily hold one type of charge and increased the concentration of the other type of free carrier in working solar cells by keeping photogenerated charges from bimolecular recombination, resulting in a reduced open-circuit voltage loss to 317 mV.

INTRODUCTION

Metal halide perovskites (MHPs) are beginning to change the photovoltaic landscape with their increasingly mature technologies.[1] The efficiency of defective polycrystalline perovskite solar cells already approaches the best single-crystalline silicon solar cells,[2–5] and the stability is quickly improving.[3,6–8] Among all the intriguing physical properties of MHPs, defect tolerance is unique, which makes this thin film technology particularly attractive, as it utilizes both solution and vapor deposition processes.[9–11] Density function theory (DFT) calculations show that many bulk point defects in MHPs either form energy states in conduction and valence bands or form shallow traps.[12] However, these point defects at the perovskite film surface and grain boundaries still behave as deep traps, which cause non-radiative recombination.[13] Several calculations showed that halide interstitials (I_i^- and I_i^+), lead vacancies (V_{Pb}), and antistites (I_{MA}) can cause deep traps in methylammonium lead triiodide ($MAPbI_3$),[14–18] and recent deep-level transient spectroscopy characterizations have implied that negatively charged iodide

Please cite this article in press as: Zhou et al., Enhancing charge-emitting shallow traps in metal halide perovskites by >100 times by surface strain, Joule (2024), https://doi.org/10.1016/j.joule.2024.10.004

interstitial (I_i^-), MA vacancy (V_{MA}^-), and MA interstitial (MA_i^+) are possible origin of deep traps in $MAPbI_3$.[19] FA_I antistites are dominant surface deep traps in FAMA-perovskites.[20] To achieve record efficiency and better stability, various surface passivation strategies have been widely developed to reduced surface trap-mediated recombination to elongate carrier recombination lifetime and increase photoluminescence quantum yield.[21–23]

Recent work has shown that there are high-density shallow traps in $MAPbI_3$ with an energy depth of less than 100 meV, and such a shallow energy depth allows shallow traps to trap charges for a period and then re-emit them back to conductive band (CB) or valance band (VB), which is different from deep traps that trap charges and cause non-radiative recombination.[24] Conventional wisdom believes that charges in the shallow traps behave similarly to free charges, which causes the defect tolerance of MHPs. However, the present theory lacks critical proof to close the logical loop. First of all, the presence of shallow traps has not been directly proven in pristine or passivated perovskites, mainly because of lack of an appropriate characterization method, despite some indirect characterizations. Most existing methods for defect characterization do not work well for shallow traps in working solar cells. The most widely applied defect characterization methods for perovskite solar cells, thermal admittance spectroscopy (TAS) or drive-level capacitance profiling (DLCP), generally only measure deep traps with a depth larger than 100 meV from the CB or VB edges.[25–27] Second, DFT calculation fails in accurate prediction when the defect energy depth is in the order of kT, where k is Boltzmann constant and T is room temperature. Third, there has been no study showing whether the charges in shallow traps really behave as free ones or should be treated differently yet.

There are very limited studies about shallow traps in MHPs. Some charge traps were treated as shallow, such as iodine interstitials, which were reported to reduce the perovskite stability,[28] but they were shown to be deep in other studies.[14,15,18] Long carrier recombination lifetimes have been occasionally observed using time-resolved microwave conductivity (TRMC), which were often attributed to shallow traps. Early analysis of $MAPbI_3$ films using TRMC derived an extremely shallow trap depth of 10 meV with low concentration in $MAPbI_3$ films, which explains the significant suppression of charge recombination.[29] A relatively long carrier recombination lifetime was observed in the $(FA, MA, Cs)Pb(I_{1-x}Br_x)_3$ films and was reduced notably after light soaking of the films. This was explained by shallow traps in the initially well-intermixed halide distributions, which converted into deep traps due to light-induced phase segregation.[30] Ultralong carrier lifetime up to 100 μs was observed in formamidinium-caesium (FACs) perovskite film with Na^+ incorporation[31]; however, such a long lifetime might not be explained by shallow trap formation. Recently, the presence of shallow traps in typical triple-cation perovskite was evidenced by extremely long-lived time-resolved photoluminescence (TRPL) measurements with a high dynamic range of greater than 10 orders of magnitude, where a high density of shallow defects dominated recombination and limited device performance.[32] However, direct studies of shallow traps in working devices are rare, and very little is known about the chemical nature, density, distribution, and the impact of solar cell performance of shallow traps, despite these understandings representing one of the fundamental ingredients for fully understanding shallow trap physics in MHPs, which may also help further improve the performance of perovskite devices.

In this work, we characterized shallow traps in working perovskite solar cell devices and found that MHPs have much richer shallow traps than traditional semiconductors, and the shallow traps are mainly located at the surface. We demonstrated that shallow trap density can be enhanced by >100 times by the surface stain, which was introduced through the fast surface reaction between formamidinium cation (FA^+) and molecules with amine at two terminals. We also showed that the high-density shallow trap can temporarily hold one type of charge and increase the density of the other type of charge by keeping them from bimolecular recombination and reduce the open-circuit voltage (V_{OC}) loss of a very stable FACs-perovskite solar cell to 317 mV, which is the best among the p-i-n perovskite solar cells.

RESULTS AND DISCUSSION

Charge-emitting shallow trap characterizations

Our recent work demonstrated a high density of shallow traps at the grain boundaries and the surface of the polycrystalline $MAPbI_3$ films,[24] where we developed a method to extract the trapping/detrapping information by directly collecting the detrapped charges in working perovskite devices. Here, we continue to develop this method to quantify the percentage of charges that are extracted without encountering charge traps, non-radiatively recombining, or being trapped and then re-emitted. The measurement system is illustrated in Figure S1, where a train of picosecond laser pulses with controlled photon number per laser pulse is shined onto perovskite solar cells, generating a known number of electron-hole pairs (N_0), which can be derived from the absorption and reflection/scattering of the devices. The read-out electronics, which include a charge-sensitive preamplifier and a shaping amplifier, convert the charges extracted to the electrodes into voltage pulses with a pulse amplitude proportional to the extracted charge numbers, and the output signal was recorded by an oscilloscope. As shown in Figure 1A, a portion of charges (N_1) is directly collected by electrodes without encountering any charge traps. Some charges are trapped by deep traps and thus are not collected by the electrodes within the measurement period. Some charges are temporarily held up by shallow traps with a delay time (Δt), and then re-emitted to the CB or VB and then collected by electrodes (N_2). The collection of these charges generates voltage pulses with heights representing the integrated charge numbers.

An output signal of a perovskite solar cell is shown in Figure 1B. For each laser excitation event, directly collected charges cause a large pulse, followed by multiple much smaller pulses with time delays caused by the detrapping of charges from shallow traps with different depths. The delay time (Δt) is related to the trap depth (E_a) based on the relationship $\frac{1}{\Delta t} = \left(\frac{\sigma v_{tl}}{g}\right) N e^{-\frac{\Delta E}{kT}}$, where σ is the electron (or hole) capture cross section, v_{tl} is the electron (hole) thermal velocity, g is the degeneracy of the trap level, N is the effective density of states in CB (or VB), ΔE is the energy separation between the trap level and CB (or VB), k is Boltzmann constant, and T is the absolute temperature.[33,34] We recorded

Please cite this article in press as: Zhou et al., Enhancing charge-emitting shallow traps in metal halide perovskites by >100 times by surface strain, Joule (2024), https://doi.org/10.1016/j.joule.2024.10.004

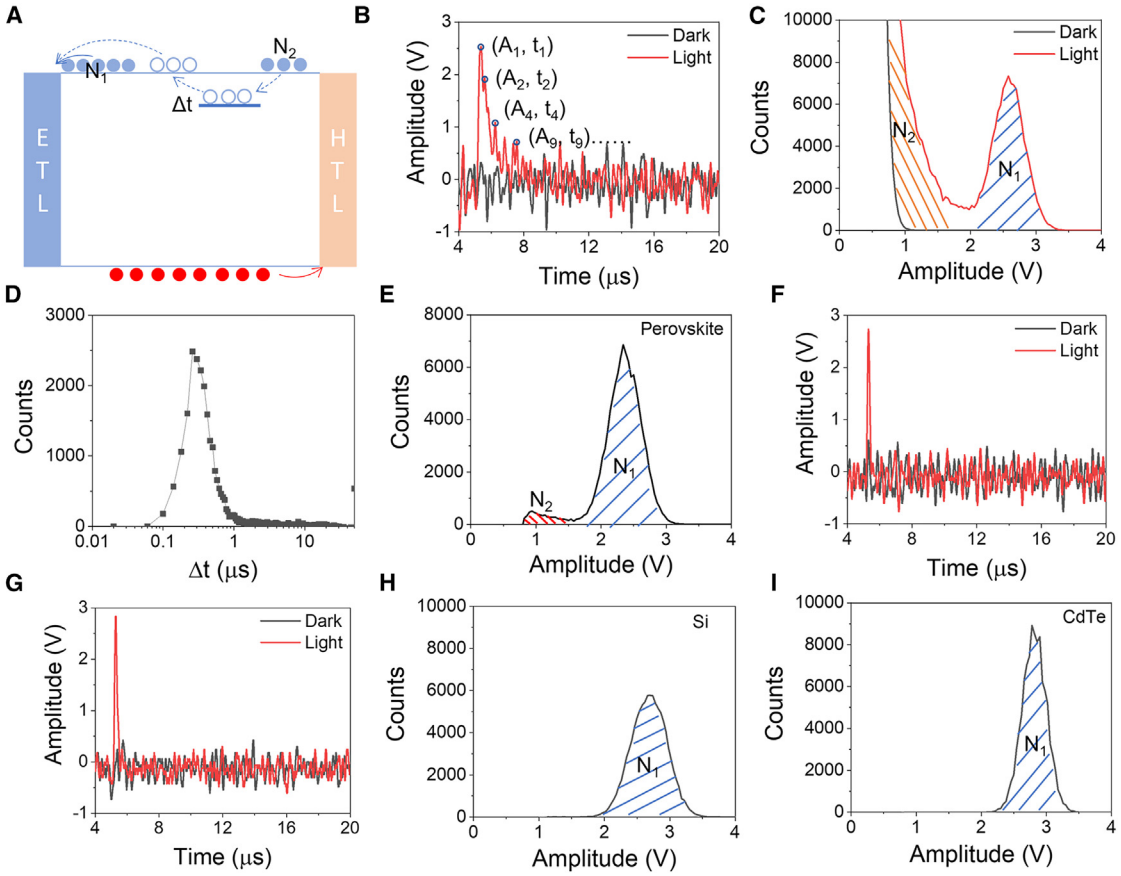

Figure 1. Charge-emitting shallow traps characterization

(A) Schematic diagram of the charge collection process in the presence of charge-emitting shallow traps.
(B) An output signal of a perovskite solar cell from the measurement setup.
(C) *N*-*A* plot derived from 50,000 output signals under laser and in dark.
(D) *N*-Δt plot of a typical perovskite solar cell.
(E) *N*-*A* plot of a typical perovskite solar cell.
(F) An output signal of the S1133 Si diode from the measurement setup.
(G) An output signal of a CdTe solar cell from the measurement setup.
(H) *N*-*A* plot of the S1133 Si diode.
(I) *N*-*A* plot of a CdTe solar cell.

the information of each pulse, including amplitude and delay time (*A*, Δt). After collecting data from 50,000 to 100,000 laser-pulse-induced events, we plotted the histogram of the pulses in amplitude domain (*N*-*A*) and delay time domain (*N*-Δt) (Figures 1C and 1D). It should be noted that the statistical method of large amounts of data can eliminate the influence of random pulses on the results, and only certain fixed-delayed pulses will be reflected as peaks in the *N*-*A* or *N*-Δt plots, because the occurrence probability of random pulses in time and amplitude is the same. By subtracting the *N*-*A* or *N*-Δt histograms of the device under laser pulses from those measured in the dark, we can exclude the background noise signal. The area below the curve represents the total number of collected charges. Then, we can derive the percentage of charges that are directly collected right after laser excitation (N_1/N_0), collected after delay (N_2/N_0), and those that are lost due to deep traps ($1 - N_1/N_0 - N_2/N_0$).

Figure 1D shows a *N*-Δt plot of a typical p-i-n perovskite solar cell with a device structure of indium tin oxide (ITO)/poly[bis(4-phenyl)(2,4,6-trimethylphenyl)amine] (PTAA)/$Cs_{0.08}FA_{0.92}PbI_3$/C_{60}/bathocuproine (BCP)/copper (Cu). This perovskite composition has been shown to be very stable with module lifetime over thousands of hours under light soaking at an open-circuit voltage condition and a temperature of 60°C ± 5°C.[3,6] We can observe many pulses after the main extraction peak with delay times of 260 ± 20 ns. The TRPL decay times derived by two-exponential fitting were τ_1 = 30 ns, τ_2 = 226 ns (Figure S2). The τ_1 was too short to be resolved by the shallow trap characterization method, and the consistency of the decay time of 226 ns in TRPL and delay time of 260 ± 20 ns in shallow trap characterization validates the shallow trap characterization method. Figure 1E shows the *N*-*A* plot of the same perovskite solar cell, where we can observe a peak with higher amplitude, which represents directly collected charges without delay, and another distinct peak at

Please cite this article in press as: Zhou et al., Enhancing charge-emitting shallow traps in metal halide perovskites by >100 times by surface strain, Joule (2024), https://doi.org/10.1016/j.joule.2024.10.004

lower amplitude side, which is attributed to the re-emitted charges with some delay. Under a photogenerated charge concentration of 4.9×10^{12} cm^{-3}, the percentages of charges that were collected directly, collected after being trapped and re-emitted, and lost by non-radiative recombination were calculated to be 38.8%, 1.8%, and 59.4%, respectively. Furthermore, the density of the charges that are re-emitted from shallow traps was estimated to be 9×10^{10} cm^{-3} from the total re-emitted charge number and perovskite volume (see experimental procedures for details). It represents a low limit for the shallow trap density because many shallow traps may not even encounter a charge. The deep traps density was estimated as 2.4×10^{12} cm^{-3} from the total recombination charge number and perovskite volume, which is 3 orders of magnitude lower than the photogenerated charge concentration used in internal quantum efficiency (IQE) measurement (10^{15} cm^{-3}). The peak IQE of typical perovskite solar cells can reach >95% in the conventional IQE measurement.[35,36]

To examine whether the presence of shallow traps in perovskite devices is general, we also fabricated perovskite devices with different perovskite compositions and hole transport layers, including ITO/PTAA/$MAPbI_3$/C_{60}/BCP/Cu, ITO/PTAA/$Cs_{0.2}FA_{0.8}Pb(I_{0.8}Br_{0.2})_3$/$C_{60}$/BCP/Cu, and FTO/$NiO_x$/$Cs_{0.1}FA_{0.9}PbI_3$/$C_{60}$/BCP/Cu, and shallow traps were detected in all these perovskite solar cells (Figure S3). The $MAPbI_3$ device showed a lower shallow trap density than the CsFA devices, which is consistent with the fact that FA-perovskites have longer carrier recombination lifetime and diffusion length than those of MA-perovskites.[37–40] The bromine-containing perovskite device showed a much higher shallow trap density and longer trapping time than the pure iodide-based perovskite device, and the device with NiO_x hole transport layer also showed a higher shallow trap density and longer trapping time than the device with PTAA hole transport layer, implying that different crystallization processes caused by the difference in compositions and interfaces also impact the shallow trap density and properties. We conducted the same characterizations on a single-crystalline silicon PIN diode (Hamamatsu S1133) and an efficient CdTe thin film solar cell.[41] In striking contrast, neither the Si diode nor the CdTe solar cell showed any delayed pulses after the strong pulse caused by directly collected charges (Figures 1F and 1G), indicating the absence of shallow charge traps in the Si, CdTe, or InGaN (Figures 1H, 1I, and S4). This again shows that perovskites are unique with their very rich shallow traps.

Increase charge-emitting shallow trap density by strain engineering

We explored several surface passivators to increase the shallow trap density, including phenethylammonium iodide (PEAI), 3-(decyldimethylammonio)-propane-sulfonate inner salt (DPSI), NaI, thiophene, diphenylphosphine, 2,7-dibromofluorene, dopamine hydrochloride, thiosemicarbazide, and p-toluenesulfonic anhydride (TSA). All devices were fabricated with a structure of ITO/PTAA/$Cs_{0.08}FA_{0.92}PbI_3$/C_{60}/BCP/Cu. However, none of them notably increased the emissive shallow trap density (Figure S5). Interestingly, we discovered that surface treatment of FA-containing perovskites using bilateral amines, such as ethylenediamine (EDA), enhanced the shallow trap density. As shown by the *N*-Δt plot in Figure 2A, the pristine device showed only one remission peak at 260 ± 20 ns. After being treated with 2 mg mL^{-1} EDA, the perovskite device had a de-trapping time of 420 ± 20 ns, whereas the reemission peak at 260 ± 20 ns was almost the same. This is consistent with the new PL decay times of the EDA-treated film, which were $\tau_1 = 0.47$ ns and $\tau_2 = 409$ ns, validating the shallow trap measurement method again (Figure S6). For each excitation laser pulse that generated 4.9×10^6 electron-hole pairs, the number of charges that were first trapped and then collected after reemission were derived from the *N*-*A* plots to be 5.6×10^3 and 6.2×10^5 in the pristine and 2 mg mL^{-1} EDA-treated devices, respectively (Figure 2B), and the total number of collected charges, including directly collected and re-emitted trapped charges, was 2.0×10^6 and 2.2×10^6 in the pristine and 2 mg mL^{-1} EDA-treated devices, respectively. This reveals that the EDA surface treatment increased the shallow trap density by 2 orders of magnitude, whereas it did not reduce the Shockley-Read-Hall (SRH) recombination. To further verify the effect of EDA in enhancing shallow trap density, we conducted cryogenic thermally stimulated photoemission spectroscopy (C-TSPS) measurement, which can also detect ultra-shallow traps.[42] This method is based on creating charge carriers by photoexcitation at low temperature and recording the thermally stimulated photoemission as a function of temperature. It is similar to thermoluminescence (TL) spectroscopy, where the emitted photons, due to the recombination of de-trapped electrons with holes in recombination centers, are detected during the temperature sweep.[43] As shown in Figure 2C, the TL intensity of re-emitted charges was enhanced by ~75 times after the film was treated by 2 mg mL^{-1} EDA. This also indicates that shallow traps mainly exist in the perovskite film surface, rather than in the charge transport layers of the perovskite solar cells.

It is interesting to find out why EDA can increase the shallow trap density in perovskites. Amines have been reported to quickly react with FA^+ on the surface of FA^+ containing perovskites even at room temperature.[44] Because EDA has amine groups at both ends, it can react with the two FA^+ cations in adjacent lattice cells and generate n′-[2-(aminomethylideneamino) ethyl]methanimidamide (2-EMA). After replacing the FA^+ cations in two adjacent unit cells with 2-EMA, the unit cells locally expanded in the direction perpendicular to the 2-EMA molecular chain (Figure 2D). The device did not show any degradation after the shallow trap measurement and the surface treatment did not change grain structure (Figure S7). The shallow traps do not introduce additional electron or hole donors; thus, they might not change the work function or band bending of the perovskite surface. The application of the bilateral amines also makes the surface of perovskite films more hydrophobic by exposing the hydrophobic chains.[45] We hypothesize that the strain is the origin of the new shallow traps based on the observation that devices without strain did not induce new shallow traps. To verify this, we treated the perovskite surface with propylamine (PA), which has a similar molecular structure to EDA but only one amine group at one end. The shallow trap reemission peak did not appear in the device with PA surface treatment (Figure 2B). We also evaluated five other molecules with only one terminal amine group. The results lead to the same conclusion that

Please cite this article in press as: Zhou et al., Enhancing charge-emitting shallow traps in metal halide perovskites by >100 times by surface strain, Joule (2024), https://doi.org/10.1016/j.joule.2024.10.004

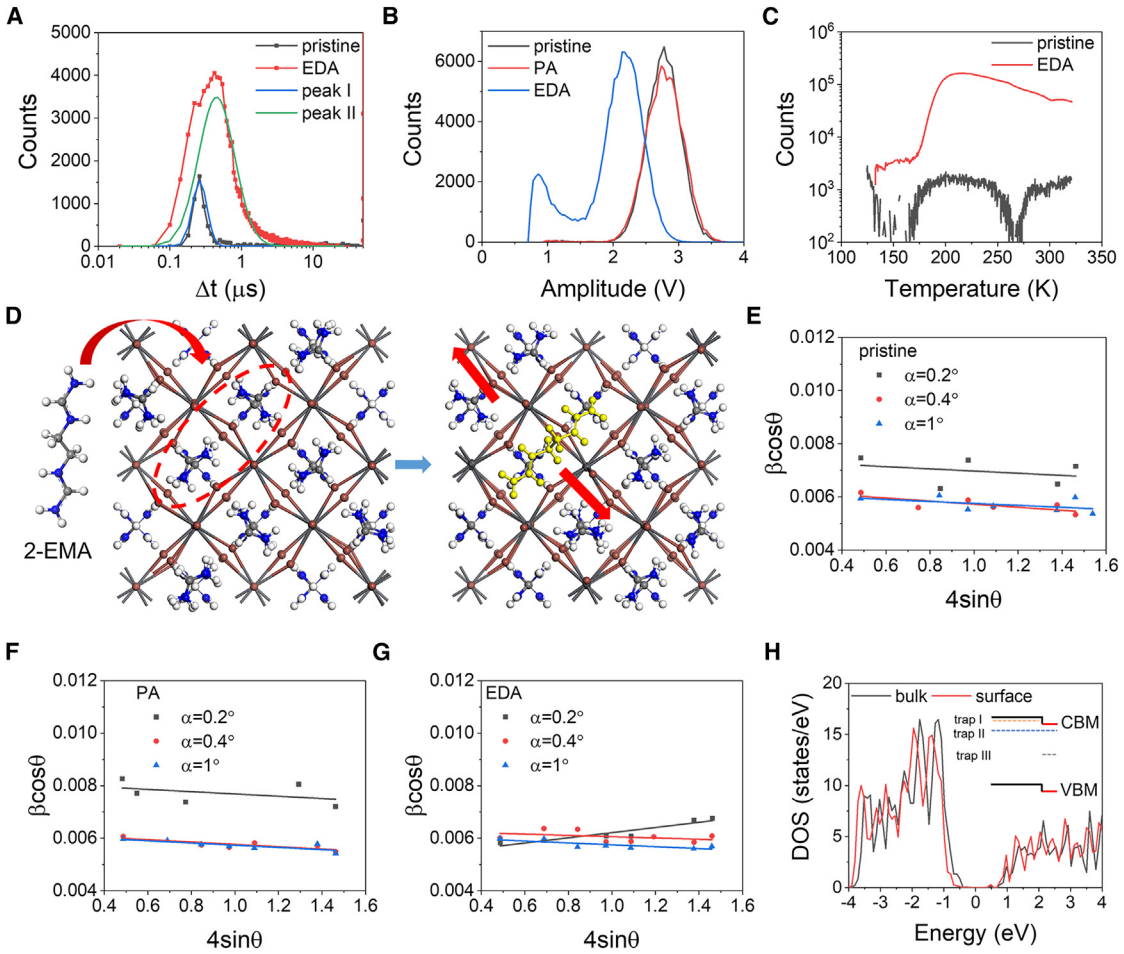

Figure 2. Shallow trap manipulation by microstrain

(A) *N*-Δt plots of the pristine and 2 mg mL^{-1} EDA-treated devices, the green and blue lines are the peaks fitting for 2 mg mL^{-1} EDA-treated devices.
(B) *N*-*A* plots of the pristine, 2 mg mL^{-1} PA-treated, and 2 mg mL^{-1} EDA-treated devices.
(C) The cryogenic thermally stimulated photoemission spectra of the pristine and 2 mg mL^{-1} EDA-treated films.
(D) Expansion of the perovskite lattice after EDA treatment.
(E–G) Williamson-Hall plot of (E) pristine, (F) 2 mg mL^{-1} PA-treated, and (G) 2 mg mL^{-1} EDA-treated perovskite films at various grazing angles.
(H) DFT calculation and band edge downshifting introduced by surface local strain.

surface treatment using molecules with one amine group at one end did not increase the shallow trap density (Figure S8).

To verify the contribution of strain to charge-emitting shallow traps, we employed the Williamson-Hall method on pristine, PA-treated, and EDA-treated films to quantify the microstrain based on the different scattering vector dependence on peak broadening in grazing incidence X-ray diffraction (GIXRD).[46] At depths of 10, 20, and 50 nm, corresponding to X-ray incident angles of 0.2°, 0.4°, and 1°,[47] the pristine and PA-treated films showed a depth-independent uniform compressive strain of −0.05% ± 0.01% and −0.04% ± 0.01% along the out-of-plane direction, respectively (Figures 2E and 2F). However, the EDA-treated film showed a depth-dependent gradient strain of 0.10% ± 0.02% at 10-nm depth, −0.03% ± 0.01% at 20-nm depth, and −0.04% ± 0.01% at 50-nm depth (Figure 2G), showing that the PA-treatment did not introduce locally expanded lattice structure, but EDA treatment inverted the surface strain.

To explore the evolution of electronic properties associated with the tensile effect on the perovskite surface, the local density of states (LDOS) across the transition from the bulk region of the perovskite to its surface were calculated using DFT. The locally expanded lattice structure on the surface can induce band edge downshifting by 0.15 eV on both the valence band maximum (VBM) and conduction band minimum (CBM) compared with those in the bulk region (Figure 2H). The band edge downshifting reduces the energy gap between defect levels and the CBM at the surface, which can reduce the energetic depth of deep traps on the surface and thus enable them to re-emit trapped charges and enhances device V_{OC}.

Combination of deep trap passivation and shallow trap enhancement to increase V_{OC}

We studied the influence of shallow traps on solar cell device performance. The pristine device had a V_{OC} of 1.070 V, and the

Please cite this article in press as: Zhou et al., Enhancing charge-emitting shallow traps in metal halide perovskites by >100 times by surface strain, Joule (2024), https://doi.org/10.1016/j.joule.2024.10.004

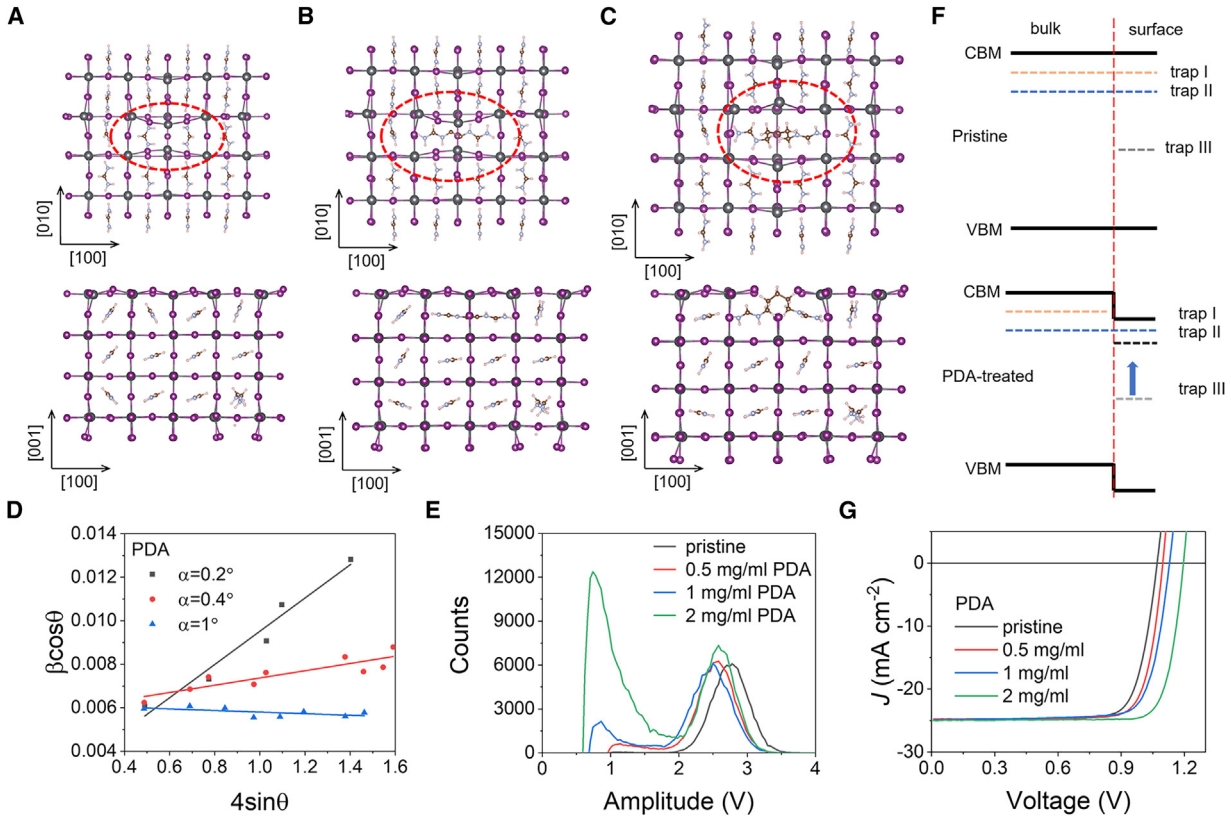

Figure 3. Passivate deep traps and introduce shallow traps simultaneously

(A) Atomic scheme of Pb-Pb dimer on (001) plane.

(B) Atomic scheme of EDA-treated perovskite (001) plane surface.

(C) Atomic scheme of PDA-treated perovskite (001) plane surface.

(D) Williamson-Hall plot of the PDA-treated films at various grazing angles.

(E) *N-A* plots of devices with PDA surface treatment with various concentration.

(F) A schematic of PDA treatment contribution on shallow trap enchantment and deep traps passivation.

(G) Typical *J-V* curves of devices with PDA surface treatment with various concentration.

V_{OC} of 2 mg mL^{-1} EDA-treated device increased to 1.133 V (Figure S9A), whereas the J_{SC} and external quantum efficiency (EQE) were almost unchanged in these devices (Figure S9B), excluding the increase in V_{OC} caused by the increased band gap (E_g). The pristine and 2 mg mL^{-1} EDA-treated devices did not show obvious hysteresis under reverse and forward scanning (Figures S9C and S9D). We also collected statistical data on the V_{OC} across more than 15 devices with and without EDA treatment, which also demonstrated that 2 mg mL^{-1} EDA surface treatment obviously increased the devices V_{OC} by enhancing the shallow trap density by 100 times, whereas the short-circuit current density (J_{SC}) and fill factor (*FF*) were comparable (Figures S9E–S9H). However the total charge collection efficiency (CCE), defined as the ratio between number of total collected charges (N_1 + N_2) and generated charges (N_0), was derived to be only 40.0% and 44.3% for the pristine and 2 mg mL^{-1} EDA-treated devices, respectively, under an excitation intensity of 4.9 × 10^{12} cm^{-3}. It is noted that this carrier concentration is much lower than that induced by 1-sun light, under which more charges can saturate the deep traps; thus, the CCE would be much higher. With increasing excitation light intensity, the proportion of recombination charges decreases, and the CCE gradually approaches the IQE, which is measured under an excited carrier density of ~10^{15} cm^{-3} (Figure S10). Nevertheless, the low CCE under weak light excitation can clearly tell that the deep traps in the perovskite were not passivated by EDA.

Iodine vacancy (V_I) behaves as shallow traps near the CB; however, Pb-Pb dimers at the surface behave as deep traps.[46] Taking the Pb-Pb dimer in (001) planes of perovskite as an example, which has the strongest XRD intensity, the formation of Pb-Pb dimers causes the local interplanar spacing along the out-of-plane [001] direction to decrease from the ideal 6.36 to 6.13 Å, which is consistent with the weak compressive strain along the out-of-plane direction in the pristine film. Because the molecular length of the reaction product of EDA and FA$^+$ in the adjacent unit cells is slightly smaller than the spacing between the two FA$^+$ cations in the two adjacent unit cells, the alkyl chain of the reaction product is almost linear between adjacent lattices and does not rotate or protrude toward the [001] direction, making it unable to separate Pb-Pb dimers

Please cite this article in press as: Zhou et al., Enhancing charge-emitting shallow traps in metal halide perovskites by >100 times by surface strain, Joule (2024), https://doi.org/10.1016/j.joule.2024.10.004

(Figures 3A and 3B). Therefore, we further explored other bilateral amines with longer alkyl chain molecules that may separate Pb-Pb dimers.

The bilateral amine 1,5-pentanediamine (PDA) has an alkyl chain longer than that of EDA. The linear molecular length for the reaction product of PDA and two FA^+ is 8.83 Å, which is much larger than the distance between the two FA^+ ions in adjacent unit cells of 6.36 Å, forcing the alkyl chain in the reaction product to rotate and protrude toward the [001] direction, occupying iodine vacancies and effectively separating the Pb dimers (Figure 3C). The space torsion configuration increases the local interplanar spacing along the [001] direction from 6.13 Å without PDA treatment to 6.28 Å after processing, corresponding to a tensile strain along an out-of-plane direction in the (001) planes. To verify this, we measured the strain in the PDA-treated film. As shown in Figure 3D, the PDA treatment introduced a larger surface tensile strain of 0.76% ± 0.01% measured at the top 10 nm, and the tensile strain reduced to 0.17% ± 0.03% at the depth of 20 nm. There was still a compressive strain of −0.04% ± 0.02% at the depth of 50 nm, which was same with the pristine film. The surface tensile strain is believed to transform the deep traps of the Pb dimer caused by V_I under compressive strain to shallow traps. To verify this, we compared the XPS spectra of I 3d and Pb 4f in the pristine, the EDA-treated, and the PDA-treated films. The I 3d peaks in these three films were located at the same binding energy (Figure S11). The binding energy of Pb 4f peaks in the EDA-treated film was same as that in pristine film, and it shifted toward higher binding energy in the PDA-treated film, demonstrating that the electron cloud overlap between Pb ions on the PDA-treated surface decreases. This indicates that the distance between Pb ions on the surface increases and Pb-Pb dimers have been separated after PDA surface treatment.[48]

We conducted the shallow trap characterization on the PDA-treated devices. The *N*-Δt plots show that the 2 mg mL^{-1} PDA-treated devices have a new trapping reemission peak centered at 740 ± 20 ns, in addition to the same trapping reemission peak of 260 ± 20 ns in the pristine devices (Figure S12A). The consistency of the TRPL decay time and the trapped time of films treated with various PDA concentrations validates the shallow trap measurement method again (Figures S12B and S12C). By integrating the *N*-*A* plot in Figure 3E, the CCE of the PDA-treated device increased to 86.0%, and the percentage of charges collected directly and after being trapped was 37.5% and 48.5%, respectively, for the PDA-treated device, implying that a high density of shallow traps was generated, and the deep traps were simultaneously passivated by PDA treatment (Figure 3F). The typical *J*-*V* curves of PDA-treated solar cells are shown in Figure 3G. The optimal devices exhibited a highest V_{OC} of 1.20 V. Because the band gap of the perovskite derived from EQE was 1.51 eV (Figures S13A and S13B), it represents 96.8% of the Shockley-Queisser limit of V_{OC} (1.24 V) for a 1.51 eV band-gap semiconductor. The corresponding V_{OC} loss (E_g-V_{OC}) was 317 mV, which is the lowest value reported among p-i-n perovskite solar cells. The 2 mg mL^{-1} PDA-treated devices did not show obvious hysteresis under reverse and forward scanning (Figure S13C) and after shallow trap measurement (Figure S13D). We collected statistical data on the V_{OC} for over 15 devices with various PDA treatment concentrations, and the data demonstrate that the devices V_{OC} increased as long as the PDA concentration increased, whereas the J_{SC} and *FF* were comparable (Figures S13E–S13H). We also evaluated five other molecules with bilateral or multiple terminal amines that have an alkyl chain longer than that of EDA, and the results come to the same conclusion that these surface treatments can simultaneously passivate deep traps and introduce shallow traps (Figure S14).

Contribution of charge-emitting shallow traps to V_{OC} enhancement

We then examined whether the presence of shallow traps would impact the device V_{OC} by modifying the established carrier dynamics rate equation with a charge trapping term and a charge detrapping term (Figure 4A)[49]:

$$\frac{dn_e}{dt} = G - R_{eh}n_e n_h - R_{SRH}n_e - R_{cap}(N_T - n_T)n_e + R_{detrap}n_T - R_{Auger}\left(n_e^2 n_h + n_e n_h^2\right) \quad \text{(Equation 1)}$$

$$\frac{dn_T}{dt} = R_{cap}(N_T - n_T)n_e - R_{detrap}n_T \quad \text{(Equation 2)}$$

$$n_h = n_e + n_T \quad \text{(Equation 3)}$$

where n_e is free-electron concentration, n_h is free-hole concentration, N_T is the shallow trap density, n_T is the population of trapped electrons in shallow traps, G is charge generation rate under continuous AM1.5G illumination, R_{Auger} is Auger recombination constant, R_{eh} is bimolecular recombination constant, R_{SRH} is deep-trap-mediated recombination constant (SRH recombination), R_{cap} is trap capture rate constant, and R_{detrap} is the rate constant of electrons reemitting back to the CB. Here, we only consider the electron shallow traps, and these three equations describe the kinetics evolution of free and trapped electron concentration, n_e and n_T, respectively. The total concentration of electrons in CB and trap states matches hole concentration n_h to keep the charge neutrality in the perovskite films.

By solving the equations numerically, we can derive the transient and equilibrium carrier concentrations (see experimental procedures for details). Figure 4B gives the evolution of free carrier concentration at a given moderate shallow trap density of N_T = 10^{15} cm^{-3}, a detrapping rate constant of R_{detrap} = 5 × 10^6 s^{-1}, and a deep-trap-mediated recombination rate of R_{SRH} = 5 × 10^6 s^{-1}. When there are no shallow traps, the equilibrium free-electron and -hole concentration are same as 1.8 × 10^{14} cm^{-3}, resulting in a quasi-Fermi-level splitting of 1.108 V under AM1.5G illumination. After introducing the electron shallow traps with a density of 10^{15} cm^{-3}, the equilibrium free-electron concentration remains at 1.8 × 10^{14} cm^{-3}, whereas the equilibrium free-hole concentration increases by 10 times to 1.2 × 10^{15} cm^{-3} due to the presence of trapped electrons with a concentration of 9.7 × 10^{14} cm^{-3} based on Equation 3. It indicates that the electron shallow traps are nearly fully occupied by electrons. Partial

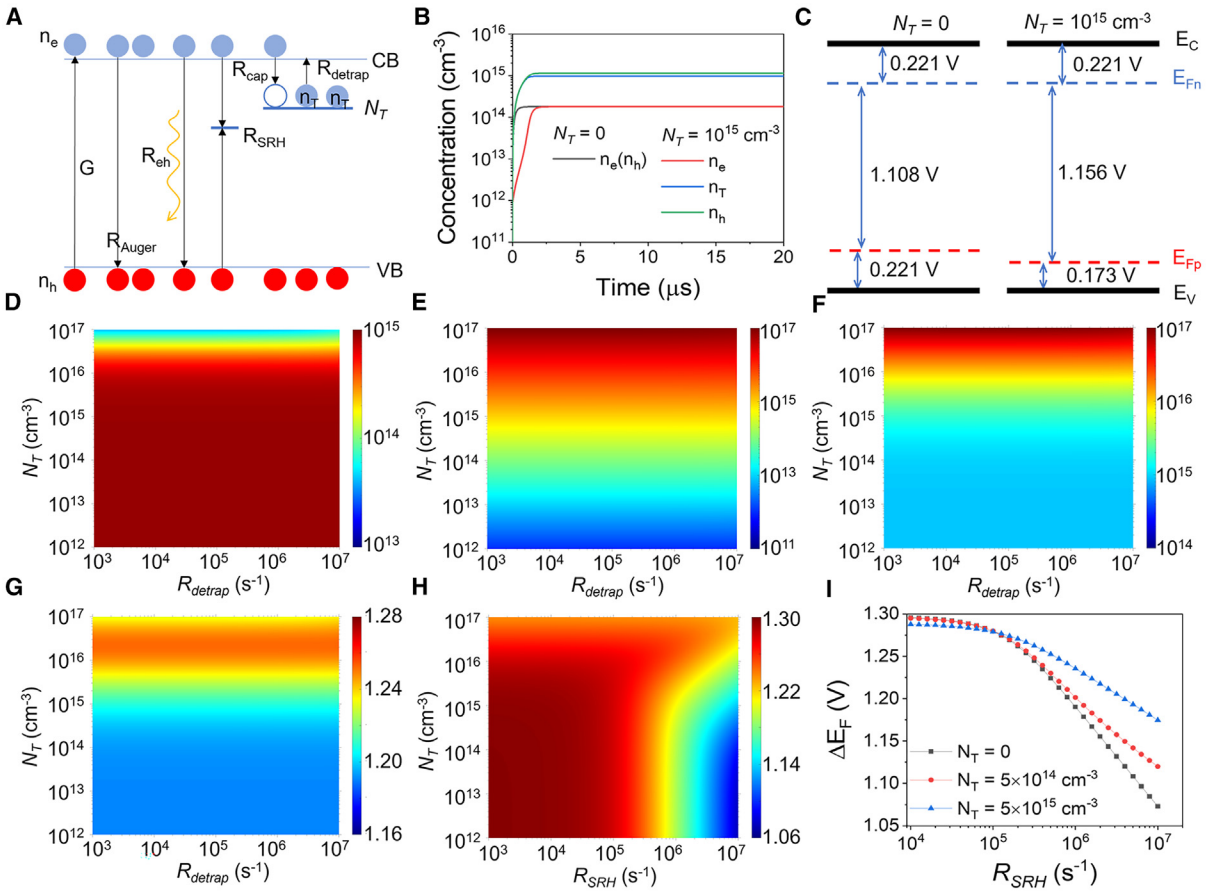

Figure 4. The impact of shallow traps on device V_{OC}

(A) Schematic of a recombination model with trapping and detrapping.

(B) Temporal carrier density with and without shallow traps.

(C) Schematic diagram of quasi-Fermi-level splitting with and without shallow traps under AM1.5G illustration.

(D–G) (D) Equilibrium free-electron concentration, (E) equilibrium trapped electron concentration, (F) equilibrium free-hole concentration, and (G) quasi-Fermi-level splitting for various shallow trap density and detrapping rate constant.

(H) Quasi-Fermi-level splitting for various shallow trap density and R_{SRH}.

(I) R_{SRH}-dependent quasi-Fermi-level splitting without and with shallow traps.

electrons are temporally held at the trap states, which leads to the reducing in bimolecular recombination and an increased free-hole concentration. Because the recombination rate in the devices is dominated by SRH recombination ($R_{SRH}n_e$), the free electrons concentration is the same regardless of emissive shallow traps. The increased free-hole concentration shifts the hole quasi-Fermi level toward VBM by 48 mV, resulting in an increase of the quasi-Fermi-level splitting to 1.156 V under AM1.5G illumination (Figure 4C). Because the quasi-Fermi levels of electrons/holes have not reached the shallow trap levels, it is unnecessary to consider the Fermi-level pinning caused by the shallow traps. It should be noted that the introduction of shallow traps does not notably affect device short-circuit current density (J_{SC}), because the trapped electrons can eventually re-emit back to CB after being delayed for some time.

To further understand the impact of shallow traps on device V_{OC}, we first investigate the contribution of shallow trap density (N_T) and trap depth (R_{detrap}) while keeping the deep-trap-mediated recombination rate (R_{SRH}) fixed at 10^6 s^{-1}. The equilibrium electron concentration, trapped electron concentration, hole concentration, and quasi-Fermi-level splitting were shown in Figures 4D–4G. When shallow trap density increases, the equilibrium free-electron concentration is unchanged, whereas the trapped electron concentration and hole concentration increased notably, leading to a gradual increase of quasi-Fermi-level splitting until the shallow trap density reaches 2.0×10^{16} cm^{-3}. The shallow traps are completely occupied by electrons, because the carrier generation rate under AM1.5G illumination is much larger than shallow trap densities we consider here.[50] Therefore, the impact of the detrapping rate constant of trapped charges on carrier concentration and the quasi-Fermi-level splitting is negligible. Further increasing the shallow trap density to above 2.0×10^{16} cm^{-3} does not further improve quasi-Fermi-level splitting. This is because

most of the photogenerated electrons are trapped by shallow traps, resulting in a decrease in the free-electron concentration. In addition, the increased free-hole concentration boosted the Auger recombination and bimolecular recombination, which further reduced the free-electron concentration. The optimal shallow trap density is around 2.0×10^{16} cm^{-3} for perovskite solar cells with a perovskite band gap of 1.55 eV to reach the largest V_{OC} of 1.25 V under AM1.5G illumination. The corresponding V_{OC} loss of 300 mV is better than the reported record performance of perovskite solar cells,[11,44,51,52] although the deep-trap-mediated recombination constant is as high as 10^6 s^{-1}.

Considering that deep trap density in perovskite films can be varied by morphology controlling and passivation, we changed shallow trap density (N_T) and R_{SRH} but kept the shallow trap detrapping rate constant (R_{detrap}) fixed at 5×10^6 s^{-1}. The equilibrium quasi-Fermi-level splitting mapping is shown in Figure 4H, and several curves of R_{SRH}-dependent quasi-Fermi-level splitting at different shallow trap densities are plotted in Figure 4I for clarification. When the R_{SRH} is smaller than 1×10^5 s^{-1}, the non-radiative charge recombination is so slow that the devices would not need the shallow traps for a large V_{OC}. With the increase of R_{SRH}, shallow traps become more important and induce a larger boost of V_{OC}. Because most reported perovskite charge recombination lifetime is less than 5 μs, or $R_{SRH} > 2 \times 10^5$ s^{-1}, shallow traps are beneficial to boost the device V_{OC}. For example, the V_{OC} can be improved by 46 mV by introducing shallow traps with a density of 5×10^{15} cm^{-3} for state-of-art perovskites with a non-radiative recombination lifetime of 1 μs.

In conclusion, we directly characterized the shallow traps in perovskite solar cells and found that MHPs are rich in shallow traps, which is different from other traditional semiconductors. The shallow traps are mainly located at the perovskite surface, and shallow trap density was enhanced by >100 times by introducing surface tensile strain. The shallow traps can temporarily hold electrons and increase free-hole concentration in working solar cells by keeping charges from bimolecular recombination and reduce the V_{OC} loss of a very stable FACs-perovskite to 317 mV, which is the best among the p-i-n perovskite solar cells. The understanding of the shallow traps in MHPs adds another aspect to the unique defect physics of perovskites, which leads to further improvement of perovskite device performance.

EXPERIMENTAL PROCEDURES

Details regarding the experimental procedures can be found in the supplemental experimental procedures.

RESOURCE AVAILABILITY

Lead contact

Further information and requests for resources and materials should be directed to and will be fulfilled by the lead contact, Jinsong Huang (jhuang@unc.edu).

Materials availability

This study did not generate new, unique materials.

Data and code availability

The authors are willing to share all the data and original code reported in the published paper with the research community. The codes are original prepared using MATLAB.

ACKNOWLEDGMENTS

We thank the financial support from National Institutes of Health under award 1R01EB033439 for the shallow trap characterization method development and measurement. The impact of shallow defects on solar cells was supported in part by Office of Basic Energy Sciences under award DE-SC0025281, and the computation is supported by the Center for Hybrid Organic Inorganic Semiconductors for Energy (CHOISE), an Energy Frontier Research Center funded by the Office of Basic Energy Sciences, Office of Science within the US Department of Energy. C-TSPS measurements were supported in part by the Center of Thermal Energy Transport under Irradiation (TETI), an Energy Frontier Research Center funded by the Office of Basic Energy Sciences, Office of Science within the US Department of Energy.

AUTHOR CONTRIBUTIONS

J.H. supervised the project. Y.Z. characterized and analyzed shallow traps. H.Z. fabricated and characterized perovskite films and devices. Y.X. and Y.Y. carried out DFT calculations. J.N.A. and F.A.S. carried out the thermoluminescence characterizations. Z.S. contributed to atomic structure. F.C., N.L., and G.Y. contributed to perovskite devices fabrication. Y.Z. and J.H. wrote the paper, and all the authors reviewed it. Y.Z. and H.Z. contributed equally to this work.

DECLARATION OF INTERESTS

The authors declare no competing interests.

SUPPLEMENTAL INFORMATION

Supplemental information can be found online at https://doi.org/10.1016/j.joule.2024.10.004.

Received: May 6, 2024
Revised: August 29, 2024
Accepted: October 2, 2024
Published: October 25, 2024

REFERENCES

1. Wilson, G.M., Al-Jassim, M., Metzger, W.K., Glunz, S.W., Verlinden, P., Xiong, G., Mansfield, L.M., Stanbery, B.J., Zhu, K., Yan, Y., et al. (2020). The 2020 photovoltaic technologies roadmap. J. Phys. D: Appl. Phys. *53*, 493001.
2. Park, J., Kim, J., Yun, H.-S., Paik, M.J., Noh, E., Mun, H.J., Kim, M.G., Shin, T.J., and Seok, S.I. (2023). Controlled growth of perovskite layers with volatile alkylammonium chlorides. Nature *616*, 724–730.
3. Fei, C., Li, N., Wang, M., Wang, X., Gu, H., Chen, B., Zhang, Z., Ni, Z., Jiao, H., Xu, W., et al. (2023). Lead-chelating hole-transport layers for efficient and stable perovskite minimodules. Science *380*, 823–829.
4. Green, M.A., Dunlop, E.D., Yoshita, M., Kopidakis, N., Bothe, K., Siefer, G., and Hao, X. (2023). Solar cell efficiency tables (version 62). Prog. Photovolt. *31*, 651–663.
5. Kim, M., Jeong, J., Lu, H., Lee, T.K., Eickemeyer, F.T., Liu, Y., Choi, I.W., Choi, S.J., Jo, Y., Kim, H.-B., et al. (2022). Conformal quantum dot–SnO_2 layers as electron transporters for efficient perovskite solar cells. Science *375*, 302–306.
6. Gu, H., Fei, C., Yang, G., Chen, B., Uddin, M.A., Zhang, H., Ni, Z., Jiao, H., Xu, W., Yan, Z., et al. (2023). Design optimization of bifacial perovskite minimodules for improved efficiency and stability. Nat. Energy *8*, 675–684.

7. Bai, S., Da, P., Li, C., Wang, Z., Yuan, Z., Fu, F., Kawecki, M., Liu, X., Sakai, N., Wang, J.T.-W., et al. (2019). Planar perovskite solar cells with long-term stability using ionic liquid additives. Nature *571*, 245–250.
8. Wang, M., Shi, Z., Fei, C., Deng, Z.J.D., Yang, G., Dunfield, S.P., Fenning, D.P., and Huang, J. (2023). Ammonium cations with high pKa in perovskite solar cells for improved high-temperature photostability. Nat. Energy *8*, 1229–1239.
9. Huang, J., Yuan, Y., Shao, Y., and Yan, Y. (2017). Understanding the physical properties of hybrid perovskites for photovoltaic applications. Nat. Rev. Mater. *2*, 1–19.
10. Liu, M., Johnston, M.B., and Snaith, H.J. (2013). Efficient planar heterojunction perovskite solar cells by vapour deposition. Nature *501*, 395–398.
11. Peng, W., Mao, K., Cai, F., Meng, H., Zhu, Z., Li, T., Yuan, S., Xu, Z., Feng, X., Xu, J., et al. (2023). Reducing nonradiative recombination in perovskite solar cells with a porous insulator contact. Science *379*, 683–690.
12. Yin, W.J., Shi, T., and Yan, Y. (2014). Unique properties of halide perovskites as possible origins of the superior solar cell performance. Adv. Mater. *26*, 4653–4658.
13. du Fossé, I., Mulder, J.T., Almeida, G., Spruit, A.G.M., Infante, I., Grozema, F.C., and Houtepen, A.J. (2022). Limits of defect tolerance in perovskite nanocrystals: effect of local electrostatic potential on trap states. J. Am. Chem. Soc. *144*, 11059–11063.
14. Du, M.-H. (2015). Density functional calculations of native defects in $CH_3NH_3PbI_3$: effects of spin–orbit coupling and self-interaction error. J. Phys. Chem. Lett. *6*, 1461–1466.
15. Meggiolaro, D., Motti, S.G., Mosconi, E., Barker, A.J., Ball, J., Andrea Riccardo Perini, C.A.R., Deschler, F., Petrozza, A., and De Angelis, F. (2018). Iodine chemistry determines the defect tolerance of lead-halide perovskites. Energy Environ. Sci. *11*, 702–713.
16. Motti, S.G., Meggiolaro, D., Barker, A.J., Mosconi, E., Perini, C.A.R., Ball, J.M., Gandini, M., Kim, M., De Angelis, F., and Petrozza, A. (2019). Controlling competing photochemical reactions stabilizes perovskite solar cells. Nat. Photonics *13*, 532–539.
17. Yin, W.-J., Shi, T., and Yan, Y. (2014). Unusual defect physics in CH3NH3PbI3 perovskite solar cell absorber. Appl. Phys. Lett. *104*, 063903.
18. Zhang, X., Turiansky, M.E., Shen, J.-X., and Van de Walle, C.G. (2020). Iodine interstitials as a cause of nonradiative recombination in hybrid perovskites. Phys. Rev. B *101*, 140101.
19. Reichert, S., An, Q., Woo, Y.-W., Walsh, A., Vaynzof, Y., and Deibel, C. (2020). Probing the ionic defect landscape in halide perovskite solar cells. Nat. Commun. *11*, 6098.
20. Wang, R., Xue, J., Chen, X., Yao, C., Wang, Z.-K., Weber, M.H., Rose, A.H., Nuryyeva, S., Zhu, J., Huang, T., et al. (2021). Unraveling the surface state of photovoltaic perovskite thin film. Matter *4*, 2417–2428.
21. Jiang, Q., Zhao, Y., Zhang, X., Yang, X., Chen, Y., Chu, Z., Ye, Q., Li, X., Yin, Z., and You, J. (2019). Surface passivation of perovskite film for efficient solar cells. Nat. Photonics *13*, 460–466.
22. Lin, R., Xu, J., Wei, M., Wang, Y., Qin, Z., Liu, Z., Wu, J., Xiao, K., Chen, B., Park, S.M., et al. (2022). All-perovskite tandem solar cells with improved grain surface passivation. Nature *603*, 73–78.
23. Aydin, E., De Bastiani, M., and De Wolf, S. (2019). Defect and contact passivation for perovskite solar cells. Adv. Mater. *31*, e1900428.
24. Zhou, Y., Fei, C., Uddin, M.A., Zhao, L., Ni, Z., and Huang, J. (2023). Self-powered perovskite photon-counting detectors. Nature *616*, 712–718.
25. Ni, Z., Bao, C., Liu, Y., Jiang, Q., Wu, W.-Q., Chen, S., Dai, X., Chen, B., Hartweg, B., Yu, Z., et al. (2020). Resolving spatial and energetic distributions of trap states in metal halide perovskite solar cells. Science *367*, 1352–1358.
26. Yang, G., Ni, Z., Yu, Z.J., Larson, B.W., Yu, Z., Chen, B., Alasfour, A., Xiao, X., Luther, J.M., Holman, Z.C., et al. (2022). Defect engineering in wide-bandgap perovskites for efficient perovskite–silicon tandem solar cells. Nat. Photonics *16*, 588–594.
27. Ni, Z., Jiao, H., Fei, C., Gu, H., Xu, S., Yu, Z., Yang, G., Deng, Y., Jiang, Q., Liu, Y., et al. (2022). Evolution of defects during the degradation of metal halide perovskite solar cells under reverse bias and illumination. Nat. Energy *7*, 65–73.
28. Tan, S., Yavuz, I., Weber, M.H., Huang, T., Chen, C.-H., Wang, R., Wang, H.-C., Ko, J.H., Nuryyeva, S., Xue, J., et al. (2020). Shallow iodine defects accelerate the degradation of α-phase formamidinium perovskite. Joule *4*, 2426–2442.
29. Oga, H., Saeki, A., Ogomi, Y., Hayase, S., and Seki, S. (2014). Improved understanding of the electronic and energetic landscapes of perovskite solar cells: high local charge carrier mobility, reduced recombination, and extremely shallow traps. J. Am. Chem. Soc. *136*, 13818–13825.
30. Guo, D., Andaji Garmaroudi, Z., Abdi-Jalebi, M., Stranks, S.D., and Savenije, T.J. (2019). Reversible removal of intermixed shallow states by light soaking in multication mixed halide perovskite films. ACS Energy Lett. *4*, 2360–2367.
31. Li, Y., Jia, Z., Yang, Y., Yao, F., Liu, Y., and Lin, Q. (2023). Shallow traps-induced ultra-long lifetime of metal halide perovskites probed with light-biased time-resolved microwave conductivity. Appl. Phys. Rev. *10*, 011406.
32. Yuan, Y., Yan, G., Dreessen, C., Rudolph, T., Hülsbeck, M., Klingebiel, B., Ye, J., Rau, U., and Kirchartz, T. (2024). Shallow defects and variable photoluminescence decay times up to 280 μs in triple-cation perovskites. Nat. Mater. *23*, 391–397.
33. Lang, D.V. (1974). Deep-level transient spectroscopy: a new method to characterize traps in semiconductors. J. Appl. Phys. *45*, 3023–3032.
34. Johnson, N.M. (1979). Energy-resolved DLTS measurement of interface states in MIS structures. Appl. Phys. Lett. *34*, 802–804.
35. Lin, Q., Armin, A., Nagiri, R.C.R., Burn, P.L., and Meredith, P. (2015). Electro-optics of perovskite solar cells. Nat. Photonics *9*, 106–112.
36. Zuo, C., Bolink, H.J., Han, H., Huang, J., Cahen, D., and Ding, L. (2016). Advances in perovskite solar cells. Adv. Sci. (Weinh) *3*, 1500324.
37. Hanusch, F.C., Wiesenmayer, E., Mankel, E., Binek, A., Angloher, P., Fraunhofer, C., Giesbrecht, N., Feckl, J.M., Jaegermann, W., Johrendt, D., et al. (2014). Efficient planar heterojunction perovskite solar cells based on formamidinium lead bromide. J. Phys. Chem. Lett. *5*, 2791–2795.
38. Pellet, N., Gao, P., Gregori, G., Yang, T.Y., Nazeeruddin, M.K., Maier, J., and Grätzel, M. (2014). Mixed-organic-cation Perovskite photovoltaics for enhanced solar-light harvesting. Angew. Chem. Int. Ed. Engl. *53*, 3151–3157.
39. Liu, M., Zhao, R., Sun, F., Zhang, P., Zhang, R., Chen, Z., and Li, S. (2022). Wavelength-tuneable near-infrared luminescence in mixed tin–lead halide perovskites. Front. Chem. *10*, 887983.
40. Zhumekenov, A.A., Saidaminov, M.I., Haque, M.A., Alarousu, E., Sarmah, S.P., Murali, B., Dursun, I., Miao, X.-H., Abdelhady, A.L., Wu, T., et al. (2016). Formamidinium lead halide perovskite crystals with unprecedented long carrier dynamics and diffusion length. ACS Energy Lett. *1*, 32–37.
41. Bista, S.S., Li, D.-B., Awni, R.A., Song, Z., Subedi, K.K., Shrestha, N., Rijal, S., Neupane, S., Grice, C.R., Phillips, A.B., et al. (2021). Effects of Cu precursor on the performance of efficient CdTe solar cells. ACS Appl. Mater. Interfaces *13*, 38432–38440.
42. Selim, F.A. (2023). Advanced thermoluminescence spectroscopy as a research tool for semiconductor and photonic materials: a review and perspective. Physica Status Solidi (a) *220*, 2200712.
43. Mackay, D.T., Varney, C.R., Buscher, J., and Selim, F.A. (2012). Study of exciton dynamics in garnets by low temperature thermo-luminescence. J. Appl. Phys. *112*, 023522.
44. Jiang, Q., Tong, J., Xian, Y., Kerner, R.A., Dunfield, S.P., Xiao, C., Scheidt, R.A., Kuciauskas, D., Wang, X., Hautzinger, M.P., et al. (2022). Surface reaction for efficient and stable inverted perovskite solar cells. Nature *611*, 278–283.

45. Wu, W.-Q., Yang, Z., Rudd, P.N., Shao, Y., Dai, X., Wei, H., Zhao, J., Fang, Y., Wang, Q., Liu, Y., et al. (2019). Bilateral alkylamine for suppressing charge recombination and improving stability in blade-coated perovskite solar cells. Sci. Adv. *5*, eaav8925.

46. Yang, B., Bogachuk, D., Suo, J., Wagner, L., Kim, H., Lim, J., Hinsch, A., Boschloo, G., Nazeeruddin, M.K., and Hagfeldt, A. (2022). Strain effects on halide perovskite solar cells. Chem. Soc. Rev. *51*, 7509–7530.

47. Dimitrievska, M., Fairbrother, A., Gunder, R., Gurieva, G., Xie, H., Saucedo, E., Pérez-Rodríguez, A., Izquierdo-Roca, V., and Schorr, S. (2016). Role of S and Se atoms on the microstructural properties of kesterite $Cu_2ZnSn(S_xSe_{1-x})_4$ thin film solar cells. Phys. Chem. Chem. Phys. *18*, 8692–8700.

48. Yang, J., Tang, W., Yuan, R., Chen, Y., Wang, J., Wu, Y., Yin, W.-J., Yuan, N., Ding, J., and Zhang, W.-H. (2020). Defect mitigation using d-penicillamine for efficient methylammonium-free perovskite solar cells with high operational stability. Chem. Sci. *12*, 2050–2059.

49. Trimpl, M.J., Wright, A.D., Schutt, K., Buizza, L.R.V., Wang, Z., Johnston, M.B., Snaith, H.J., Müller-Buschbaum, P., and Herz, L.M. (2020). Charge-carrier trapping and radiative recombination in metal halide perovskite semiconductors. Adv. Funct. Mater. *30*, 2004312.

50. Wolff, C.M., Bourelle, S.A., Phuong, L.Q., Kurpiers, J., Feldmann, S., Caprioglio, P., Marquez, J.A., Wolansky, J., Unold, T., Stolterfoht, M., et al. (2021). Orders of recombination in complete perovskite solar cells – linking time-resolved and steady-state measurements. Adv. Energy Mater. *11*, 2101823.

51. Jeong, M., Choi, I.W., Go, E.M., Cho, Y., Kim, M., Lee, B., Jeong, S., Jo, Y., Choi, H.W., Lee, J., et al. (2020). Stable perovskite solar cells with efficiency exceeding 24.8% and 0.3-V voltage loss. Science *369*, 1615–1620.

52. Li, Z., Li, B., Wu, X., Sheppard, S.A., Zhang, S., Gao, D., Long, N.J., and Zhu, Z. (2022). Organometallic-functionalized interfaces for highly efficient inverted perovskite solar cells. Science *376*, 416–420.